*Clays and Clay Minerals*, 1969, Vol. 17, pp. 83–93. Pergamon Press. Printed in Great Britain

# RHEOLOGICAL MODEL STUDIES IN CLAY

**R. W. CHRISTENSEN and J. S. KIM**
Department of Engineering Mechanics, University of Wisconsin, Madison, Wisconsin

(*Received* 12 *December* 1968)

**Abstract**—The process of deformation in clays is visualized as the combination of recoverable deformation resulting from bending and rotation of individual particles and irrecoverable deformation due to relative movement between adjacent particles at their points of contact. The relative movement between particles is treated as a rate process in which interparticle bonds are continually broken and reformed as the deformation proceeds. Accordingly, the rate of deformation is governed by the activation energy associated with the rupture of interparticle bonds. Thus, in terms of a rheological model, the fundamental element consists of a spring, representing the recoverable deformation, in series with a rate process dashpot representing the irrecoverable deformation.

Owing to the heterogeneous nature of the fabric of clay soils, i.e. varying particle size, shape, orientation, surface characteristics, etc., a wide range of activation energies, elastic stiffness, and other material properties is anticipated. This is accounted for by assuming a Gaussian distribution for the model properties. Thus, the complete rheological model postulated in this study consists of a combination of spring and dashpot elements covering the complete spectrum of model properties.

The response of the rheological model is analyzed for creep and constant strain-rate loading. The analysis is accomplished numerically using a digital computer since no closed form solution exists for the non-linear systems of equations that result from this model. Experimental data for a number of triaxial tests on clays under various conditions of loading are presented for comparison with the model behavior.

## INTRODUCTION

THE DEFORMATIONAL response of clays to applied loads is a highly complex phenomenon. A large number of physical variables influence the microscopic deformation processes, such as clay fabric, moisture content, adsorbed cations, temperature and stress history. Therefore, the task of devising a rheological model for clays in which the model parameters are specifically related to the microscopic deformation phenomena is a formidable one indeed.

One of the first attempts to formulate a rheological model for clays in which the model elements represented specific microscopic behavior was that of Geuze and Tan (1953). This model was composed of elastic springs representing bending and rotation of particles and linear dashpots representing the breaking and reforming of interparticle bonds. A few years later, Murayama and Shibata (1958) introduced the concept of rate process theory (Glasstone, Laidler and Eyring, 1941) in connection with the breaking and reforming of interparticle bonds. Recently, the rate process theory has been utilized in a number of studies of clay behavior under load (Mitchell 1964, Christensen and Wu, 1964, Mitchell *et al.*, 1968). Although the rate process hypothesis cannot be completely validated since microscopic processes are involved, these studies present very convincing evidence for rate process theory as a physical interpretation of inelastic deformation.

However, it has been pointed out (Singh and Mitchell, 1968) that all the rheological models proposed to data, have failed in some major respect to fully describe clay behavior. It is the purpose of this study to attempt to formulate an improved rheological model based upon considerations of the physico-chemical properties and fabric of clays.

## INELASTIC DEFORMATION OF CLAYS AS A RATE PROCESS

It has been demonstrated (Rosenquist, 1959; West, 1965) that the fabric of clays consists of individual particles or packets of particles arranged more or less randomly with edge-to-face contacts between particles pre-dominating. Although the exact nature of the interparticle contacts is not known, i.e. whether the contact is mineral-to-mineral or mineral through adsorbed layer to mineral, it is generally agreed that physico-chemical bonds are formed at the contacts which are partly responsible for the shearing resistance of clays. Of course, additional shearing resistance may be developed from purely mechanical phenomena such as bending and crushing of particles and volume expansion during shear.

The theory of rate processes, first advanced by



https://doi.org/10.1346/CCMN.1969.0170206 Published online by Cambridge University Press

Glasstone, Laidler, and Eyring (1941) has been used with good success to describe the behavior of such diverse materials as steel (Kauzmann, 1941) and textiles (Eyring and Halsey, 1948) as well as clays. Mitchell *et al.*(1968) have recently presented the results of a comprehensive study of creep in clays which support the rate process hypothesis. Based on its success in previous studies of clays, the rate process theory for inelastic deformation in clays is adopted in this study. Complete derivations of the theory are available in other sources (see, e.g. Tobolsky, Powell and Eyring, 1943). Therefore, only a brief outline will be presented here.

The rate process theory is based on assumption that the energy distribution over the "flow units" (atoms, molecules, or groups of molecules) can be expressed by the Maxwell-Boltzman distribution,

$$p \sim e^{-\Delta F/RT} \tag{1}$$

where $\Delta F$ is the necessary energy per mole that must be supplied for the flow unit to become "activated" and $p$ is the probability of achieving it; $R$ is the universal gas constant and $T$ is the temperature in Kelvin units. The mean frequency of thermal oscillations of the flow units is, according to statistical mechanics, $kT/h$, in which $k$ is Boltzmann's constant and $h$ is Planck's constant. Thus, the rate, or frequency, of activation of the flow units in the absence of external forces is

$$\nu = \frac{kT}{h} e^{-\Delta F/RT}. \tag{2}$$

If an external force is applied to the flow unit, an energy gradient will be created in the direction of the force, increasing the frequency of activation in the direction of the force and decreasing it in the opposite direction. The net frequency of activation in the direction of the force thus becomes

$$\vec{\nu} - \overleftarrow{\nu} = 2\frac{kT}{h} e^{-\Delta F/RT} \sinh\left(\frac{f\lambda}{2kT}\right) \tag{3}$$

in which $f$ is the applied force and $\lambda$ is the distance between the equilibrium positions of the flow units. This process can be visualized by means of the diagram shown in Fig. 1. The activation energy, $\Delta F$, is depicted as a symmetrical energy barrier in the absence of external forces which becomes distorted when an external force is applied. The distortion of the energy barrier gives rise to the net frequency of activation expressed in Eq. (3).

## A DISTRIBUTED-PARAMETER MODEL FOR CLAY DEFORMATION

In the present development, the basic unit of deformation is assumed to consist of a bond rupture, controlled by rate processes as described in the previous section, along with the associated elastic deformation. A bond is considered to be the net physico-chemical attraction between adjacent clay particles at their points of contact and may involve atoms, molecules, or groups of molecules. In order to convert the net frequency of bond rupture, as given in Eq. (3), into a macroscopic strain rate, it is necessary to introduce a structural factor $X$ so that the strain rate may be written as

$$\dot{\gamma} = X\frac{kT}{h} e^{-\Delta F/RT} \sinh\frac{\tau\lambda}{2NkT} \tag{4}$$

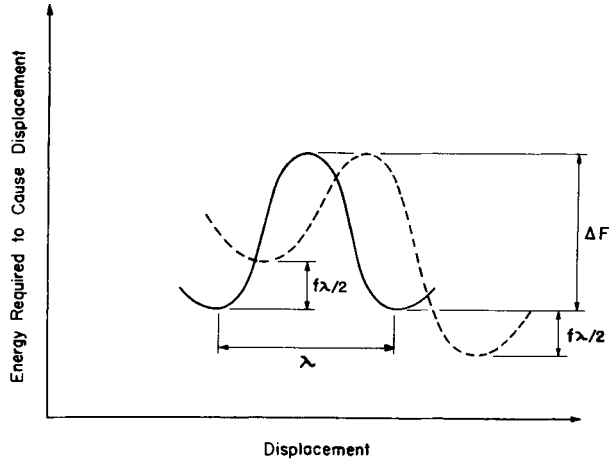



Fig. 1. The concept of energy barriers in rate process theory.

https://doi.org/10.1346/CCMN.1969.0170206 Published online by Cambridge University Press

since, $\tau = Nf$ (4a)

in which $\tau$ = macroscopic shear stress on the plane of flow
$N$ = number of bonds per unit area in the plane of flow
and $X$ = macroscopic shear strain resulting from a bond rupture.

The behavior of the basic deformation unit may thus be represented by a spring, representing the recoverable deformation, in series with a non-linear dashpot obeying Eq. (4), representing the irrecoverable deformation.

*Fundamental parameters of deformation units*

The clay mass as a whole is a complex assemblage of particles of various sizes, shapes and orientations. Therefore, it is unlikely that the characteristics of the deformation units will all be the same. In fact, it is more likely that a broad spectrum of characteristics will be found, distributed more or less at random throughout the mass. This suggests that a realistic rheological model for clay should consist of an assemblage of elements having a broad range of properties.

The basic deformation unit has four fundamental parameters; they are as follows:

(1) activation energy, $\Delta F_i$
(2) macroscopic strain resulting from bond rupture, $X_j$
(3) elastic stiffness, $K_k$
(4) ratio of strain in a deformation unit to the macroscopic strain, $\Delta_l$.

The four fundamental parameters listed are independently subscripted since, in general, one parameter for a given unit does not depend on any of the others. The first three parameters have already been defined but the last one requires further explanation. The quantity $\Delta_l$ reflects the degree of participation of a given unit in the deformation process; i.e.

$$\Delta_l = \frac{\gamma_{ijkl}}{\gamma} \tag{5}$$

where, $\gamma_{ijkl}$ = strain in a particular deformation unit
$\gamma$ = macroscopic strain in clay mass.

The quantity $\lambda$ is generally considered to be a function of the surface characteristics (Mitchell, 1965) and, as such, probably varies only slightly; therefore, it is not included among the subscripted parameters. The rheological model can thus be visualized as a number of individual elements connected in parallel as shown in Fig. 2. However, it also has the additional provision that the strain in any given element may be different from the imposed macroscopic strain as indicated by the curved dashed line.

*Assumed distributions of fundamental parameters*

The values of the parameters will depend upon the combined effects of particle size, shape and orientation, properties of the pore fluid, stress history, temperature, etc. Moreover, the distribution of these values in any given clay mass is not known and cannot be determined by presently available experimental techniques. Lacking any information to the contrary, it seems reasonable to assume that the distribution of each of the parameters considered is random.

The assumption of randomness leads to a Gaussian, or normal, distribution which is described

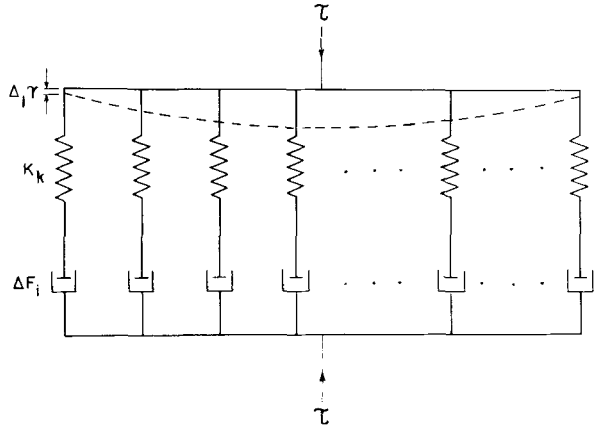



Fig. 2. The distributed-parameter model for clays.

https://doi.org/10.1346/CCMN.1969.0170206 Published online by Cambridge University Press

mathematically by the following equation:

$$P(x) = \frac{1}{S_x\sqrt{2\pi}} e^{-(x-\bar{x})^2/2S_x^2} \tag{6}$$

where, $P(x)$ is the probability that a quantity, whose mean value is $\bar{x}$, will have a value of $x$, and $S_x$ is the standard deviation. It may be noted that only two properties, the mean value and standard deviation, are required to completely define the normal distribution. A typical normal distribution curve, which could represent the distribution of any of the four parameters considered in this discussion, is shown in Fig. 3.

Thus, the rheological model shown schematically in Fig. 2, in which the parameters, $\Delta F_i$, $X_j$, $K_k$, and $\Delta_l$ are assumed to have normal distributions as shown in Fig. 3, and expressed mathematically in Eq. (6), constitutes the proposed distributed-parameter model for clays.

## RESPONSE CHARACTERISTICS OF DISTRIBUTED-PARAMETER MODEL

From Fig. 2, it can be seen that the fraction of the stress carried by the elements of the *ijkl* type is

$$\tau_{ijkl} = K_k(\gamma_{ijkl} - \gamma_{ij}) = K_k(\Delta_l\gamma - \gamma_{ij}) \tag{7}$$

where, $\gamma_{ijkl}$ is the total strain in the elements of *ijkl* type and $\gamma_{ij}$ is the strain in the dashpots of *ij* type.

The sum of the stresses carried by the individual elements is

$$\tau = \sum_{ijkl} \tau_{ijkl} \cdot n_{ijkl} \tag{8}$$

where, $n_{ijkl}$ is the fraction of the elements that are of the *ijkl* type. Summation, rather than integration, over the distribution is indicated because the response equations which follow are impossible to integrate except by numerical means. Taking the time derivative of Eq. (7) and substituting for $\dot{\gamma}_{ij}$ from Eq. (4) gives

$$\dot{\tau}_{ijkl} = K_k[\Delta_l\dot{\gamma} - \beta_{ij}\sinh(\alpha\tau_{ijkl})] \tag{9}$$

where, $\alpha = \frac{\lambda}{2NkT}$ (9a)

and $\beta_{ij} = X_j\frac{kT}{h}e^{-\Delta F_i/RT}$ (9b)

*Constant strain rate*

To obtain the response under constant strain rate loading ($\dot{\gamma}$ = constant), Eq. (9) is integrated with the initial condition

$$\tau_{ijkl} = 0 \text{ at } t = 0$$

and the resulting stresses $\tau_{ijkl}$ are summed for all the elements yielding

$$\tau = \frac{1}{\alpha}\sum_{ijkl} n_{ijkl}\log\left[\frac{\Delta_l\dot{\gamma}}{\beta_{ij}} + \frac{\sqrt{(\beta_{ij}^2 + (\Delta_l\dot{\gamma})^2)}}{\beta_{ij}}\right.$$
$$\left.\tanh\left\{\sqrt{(\beta_{ij}^2 + (\Delta_l\dot{\gamma})^2)}Z_K(t) + \tanh^{-1}\right.\right.$$
$$\left.\left.\left(\frac{\beta_{ij} - \Delta_l\dot{\gamma}}{\sqrt{(\beta_{ij}^2 + (\Delta_l\dot{\gamma})^2)}}\right)\right\}\right] \tag{10}$$

where, $Z_k(t) = \frac{\alpha}{2}K_k t.$ (10a)

Equation (10) is evaluated numerically with a digital computer and an example of the typical behavior

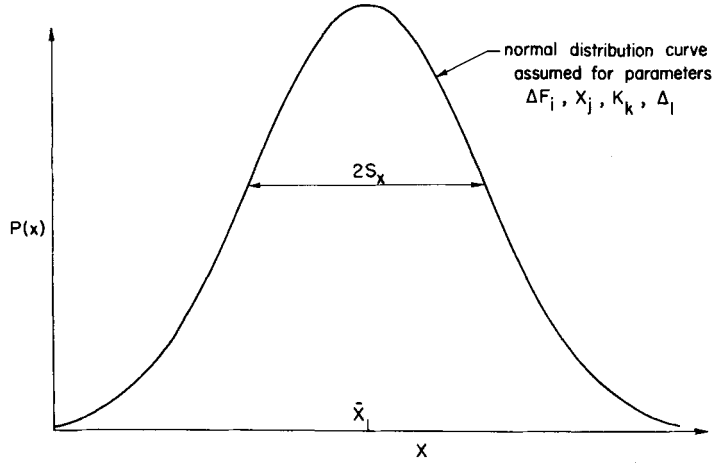



Fig. 3. Assumed normal distribution for model parameters.

https://doi.org/10.1346/CCMN.1969.0170206 Published online by Cambridge University Press

of the model under constant strain rate loading is shown in Fig. 4 for several strain rates.

The steady-state condition for this type of loading is easily obtained from Eq. (9) by setting $\tau_{ijkl} = 0$ and summing over all elements. Thus, the steady-state shear stress can be written

$$\tau_{ss} = \frac{1}{\alpha} \sum_{ijkl} n_{ijkl} \sinh^{-1}\left[\frac{\Delta_l \dot{\gamma}}{\beta_{ij}}\right]. \tag{11}$$

*Creep response*

The response of the model to creep loading is obtained by substituting Eq. (7) into Eq. (8), taking the time derivative, and setting $\dot{\tau} = 0$ which gives

$$\dot{\gamma} \sum_{ijkl} n_{ijkl} \Delta_l K_k = \sum_{ijkl} n_{ijkl} K_k \dot{\gamma}_{ij}. \tag{12}$$

However, since

$$\sum_{ijkl} n_{ijkl} \Delta_l K_k = \bar{K} \tag{13}$$

where $\bar{K}$ is the mean elastic stiffness, the equation for creep, from Eq. (12), becomes

$$\dot{\gamma} = \frac{1}{\bar{K}} \sum_{ijkl} n_{ijkl} \beta_{ij} K_k \sinh(\alpha \tau_{ijkl}) \tag{14}$$

where the $\tau_{ijkl}$ are determined by integrating the following system of non-linear differential equations resulting from the substitution of Eq. (14) into Eq. (9):

$$\dot{\tau}_{ijkl} = \frac{K_k \Delta_l}{\bar{K}} \sum_{ijkl} n_{ijkl} \beta_{ij} K_k \sinh(\alpha \tau_{ijkl}) - K_k \beta_{ij} \sinh(\alpha \tau_{ijkl}). \tag{15}$$

The numerical solution of Eq. (15) is difficult and consumes large amounts of computer time; accordingly, an alternative method was adopted to obtain the creep curves. This alternative method makes use of the constant strain rate solution which is comparatively easy to obtain. Specifically, the creep response is obtained by constructing a horizontal line corresponding to the desired stress level over a family of constant strain rate curves as shown in Fig. 4 and noting the values of strain-rate and the time parameter $Z(t)$ at the intersections.

## COMPARISON OF MODEL BEHAVIOR WITH EXPERIMENTAL RESULTS

*Material*

The soil used in this study is a commercially produced illite called Grundite. This soil has a liquid limit of about 70 per cent and a plasticity index of about 40 per cent; approximately 65 per cent by weight is finer than 2 $\mu$.

The test specimens were made by remolding at a water content of 45 per cent and trimming to standard triaxial size of 1·4 in. diameter and 3·0 in. length. They were then sealed in rubber membranes, and stored under water for one week prior to testing to eliminate thixotropic hardening effects.

*Shear tests*

Specimens were tested under conditions of constant strain rate and constant load (creep). All tests reported herein were conducted under undrained conditions. The constant strain rate tests were conducted as unconfined compression

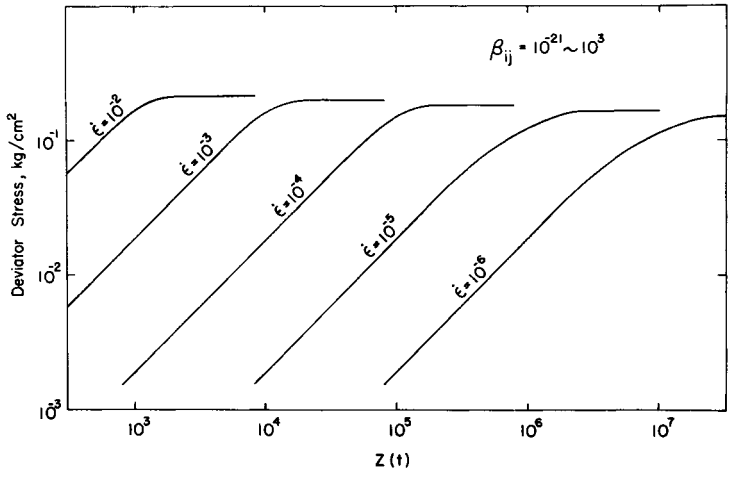



Fig. 4. Typical constant strain rate response of distributed-parameter model.

https://doi.org/10.1346/CCMN.1969.0170206 Published online by Cambridge University Press

tests in an apparatus with a controlled rate of feed. Results of 18 tests are reported with axial strain rates ranging from $1{\cdot}07 \times 10^{-3}\,\text{min}^{-1}$ to $1{\cdot}35 \times 10^{-2}\,\text{min}^{-1}$.

The creep tests were performed by applying a constant load to the specimen through a hanger arrangement. Although several creep tests have been performed as part of this study, just one typical result is shown herein. The results of the creep tests tended to be very reproducible and the typical case presented can be considered representative of all the creep tests that were performed.

## RESULTS

According to the previous discussion, there are four distributed parameters to consider: $\Delta F_i$, $X_j$, $K_k$, and $\Delta_l$. However, $\Delta F_i$ and $X_j$ always appear together in the expression for $\beta_{ij}$ as given in Eq. (9b). Therefore, a single distribution describing $\beta_{ij}$ is sufficient to take care of both $\Delta F_i$ and $X_j$. Since $\beta_{ij}$ is dominated by the term, exp $(-\Delta F_i/RT)$, logarithm of $\beta_{ij}$ is assumed to be normally distributed as shown in Fig. 5 in which $\bar{\beta}$ is the mean value.

Several distributions were tried for $K_k$ but the results indicated that the response is substantially unaffected by variations in $K_k$. This is apparently due to the dominating influence of the distribution of $\beta_{ij}$. Similarly, variations in $\Delta_l$ do not appear to affect the overall response to any significant degree. Therefore, the only distribution that must be considered is that of $\beta_{ij}$; $K_k$ and $\Delta_l$ may be treated as constants.

*Constant strain rate tests*

For purposes of comparison with the theoretical behavior of the distributed-parameter model, the constant strain rate tests are first analyzed from the standpoint of steady-state behavior. The steady-state condition is interpreted to be the shear stress and strain rate at the point where the stress-strain curve levels off. In some cases the stress-strain curve reached a peak and then dropped off; in these cases, the peak value was selected as steady-state, the drop off being attributed to failure occuring on isolated shear planes.

The steady-state results are presented in terms of "deviator stress," $D$, which is the difference between principal stresses $(\sigma_1 - \sigma_3)$, and the axial strain rate $\dot{\epsilon}$. The analogous terms in the theoretical response equations are the shear stress, $\tau$, and the shear strain rate, $\dot{\gamma}$, which are interpreted in this study as the shear stress and strain rate respectively on the octahedral plane. Christensen and Wu (1964) have shown that, under triaxial loading conditions, these quantities are related as follows:

$$\tau_{\text{oct}} = \frac{\sqrt{2}}{3} D \tag{16}$$

$$\gamma_{\text{oct}} = \sqrt{2}\,\epsilon. \tag{16a}$$

Hereafter the subscripts on $\tau$ and $\gamma$ will be omitted with the understanding that they refer to the octahedral plane.

In Fig. 6 are shown the results of 18 constant strain rate tests with the steady-state deviator

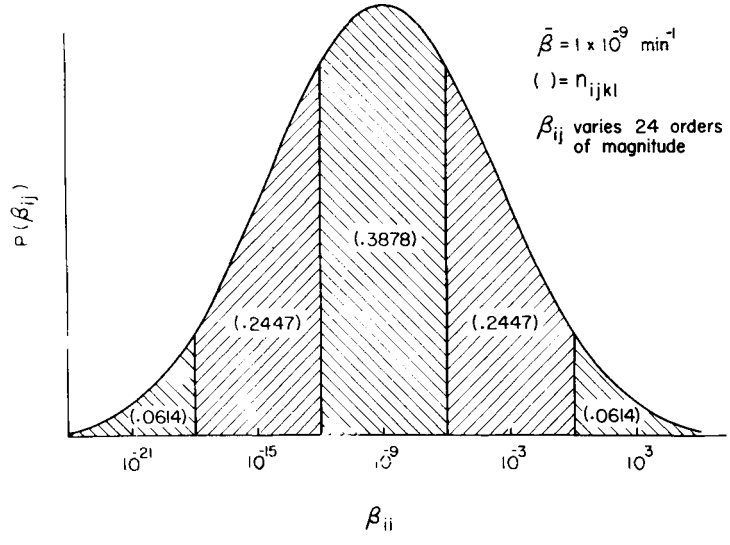



Fig. 5. Typical assumed distribution for $\beta_{ij}$.

https://doi.org/10.1346/CCMN.1969.0170206 Published online by Cambridge University Press

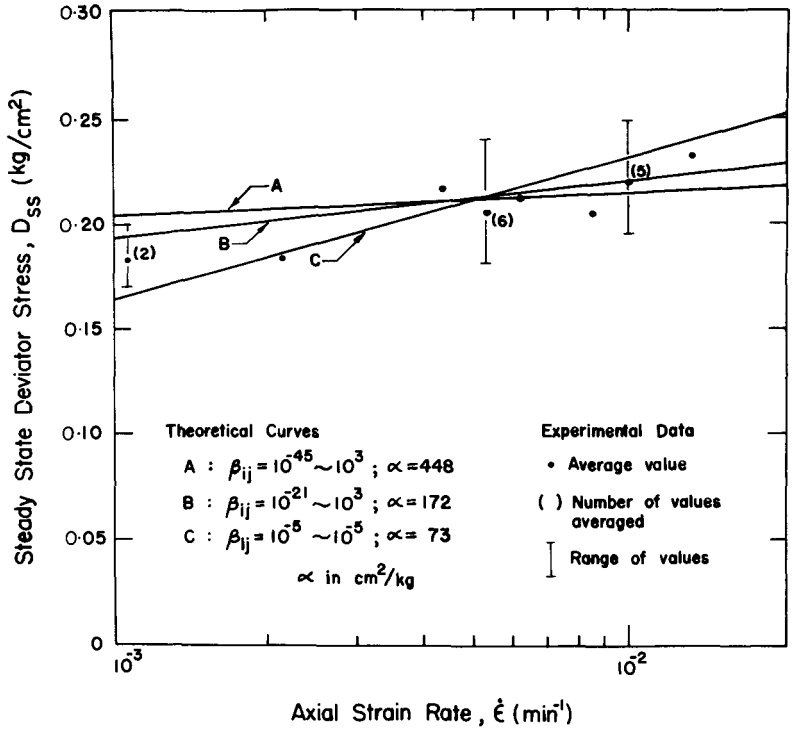



Fig. 6. Steady-state constant strain rate response.

stress, $D_{ss}$, plotted v.s. strain rate on a log scale. Although the scatter is considerable, the tendency for increasing strength with increased strain rate is readily apparent.

The theoretical curves shown in Fig. 6 are obtained from Eq. (11) by assuming a distribution of $\beta_{ij}$ and choosing $\alpha$ so as to obtain the best possible fit with the experimental data. In all cases, $\Delta_l$ is taken to be unity. The parameters $\beta_{ij}$ which were used in Fig. 6 are considered to represent the complete range of physically reasonable possibilities. It can be seen from Eq. (9b) that $\beta_{ij}$ depends on $X_j$ and $\Delta F_i$. It seems unlikely that the structural factor $X_j$ will vary more than, say, from 0·1 to 10·0 with an average of approximately 1·0. The decision as to what is a reasonable range of $\Delta F_i$ is based on two criteria: (1) no negative values of activation energy were permitted, and (2) the mean value of activation energy was not allowed to exceed 50 Kcal mole$^{-1}$. These restrictions, taken together, require $\beta_{ij}$ to fall within the range of $10^{-45}$ min$^{-1}$–$10^{15}$ min$^{-1}$. Curve A represents one extreme, where $\beta_{ij}$ is given a very large range of values, while curve C shows the opposite extreme where $\beta_{ij}$ is the same for all units. Curve B represents a case half way between *A* and *C*. It should be pointed out that these three curves do not represent all the possible combinations of $\beta_{ij}$ that can be made to fit the experimental data; however, these cases are representative and cover the complete range of behavior within the restrictions previously mentioned.

The theoretical constant strain rate response is presented in the form of dimensionless shear stress $\tau^*$ vs. the time parameter $Z(t)$ on a log scale. The dimensionless shear stress $\tau^*$ is the ratio of the actual shear stress at any time to the steady-state value; thus,

$$\tau^* = \frac{\tau}{\tau_{ss}} \tag{17}$$

where $\tau$ is given by Eq. (10) and $\tau_{ss}$ is given by Eq. (11).

Figure 7 shows several combinations of $\beta_{ij}$, the steady-state behavior of which fits the experimental data well enough to be considered as possibilities. These various combinations of $\beta_{ij}$ are grouped according to the range of $\beta_{ij}$; thus, in Fig. 7a are shown three curves for constant $\beta_{ij}$, in Fig. 7b are three curves for range of $\beta_{ij}$ of 24 orders of magnitude, and Fig. 7c shows three

https://doi.org/10.1346/CCMN.1969.0170206 Published online by Cambridge University Press

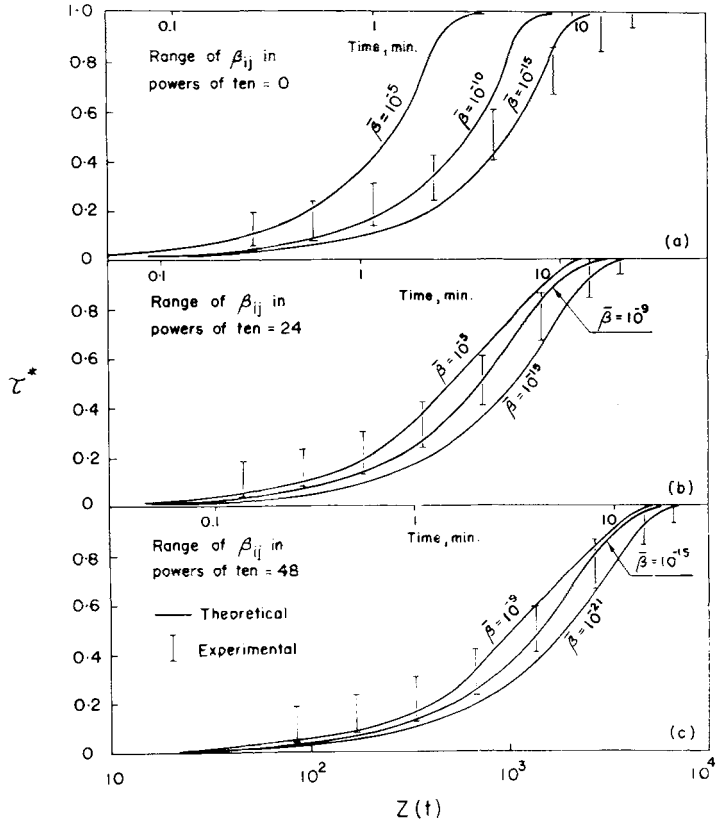



Fig. 7. Comparison of theoretical and experimental constant strain rate response.

curves for a range of $\beta_{ij}$ of 48 orders of magnitude.

Superimposed on the theoretical curves are the data for six tests. Instead of individual data points, a bar is used to show the variation of the experimental data. The real time scale corresponding to the experimental data is shown along the top of the diagram. The superposition of the data was accomplished by sliding a sheet containing the data horizontally over the theoretical curves until the best possible match was obtained. By matching the real time and the time parameter $Z(t)$, a value for $Z(t)$ is obtained. In this case

$$Z(t) \doteqdot 180 \sim 330t.$$

It can be seen from Fig. 7 that the agreement between the theoretical and experimental constant strain rate response is quite good for the cases where $\beta_{ij}$ varies over 24 and 48 orders of magnitude, although in the lower $\tau^*$ range the data tend to lie generally above the theoretical curves. However, the degree of confidence in the lower points is much less than that of the higher points because of seating difficulties when the load is first applied and because of the sensitivity of the time scale in that range. The case where $\beta_{ij}$ is a constant (Fig. 7a) does not agree well with the experimental data. If individual test results are compared with the theoretical curves, the fit is clearly superior for $\beta_{ij}$ varying over 24 or 48 orders of magnitude as compared to $\beta_{ij}$ constant. This seems to support the concept of distributed parameters. However, individual test results are not shown because of space limitations.

*Creep tests*

The theoretical creep response for the model was evaluated for the same distribution of parameters as was found to be applicable for constant strain rate. The theoretical curves are shown in Fig. 8 with the axial strain rate, $\dot{\epsilon}$, plotted versus the time parameter, $Z(t)$, on a log-log scale for a stress level of $\tau = 0{\cdot}043$ kg/cm$^2$.

Superimposed upon the theoretical curves are the data points for a typical creep test run at the

https://doi.org/10.1346/CCMN.1969.0170206 Published online by Cambridge University Press

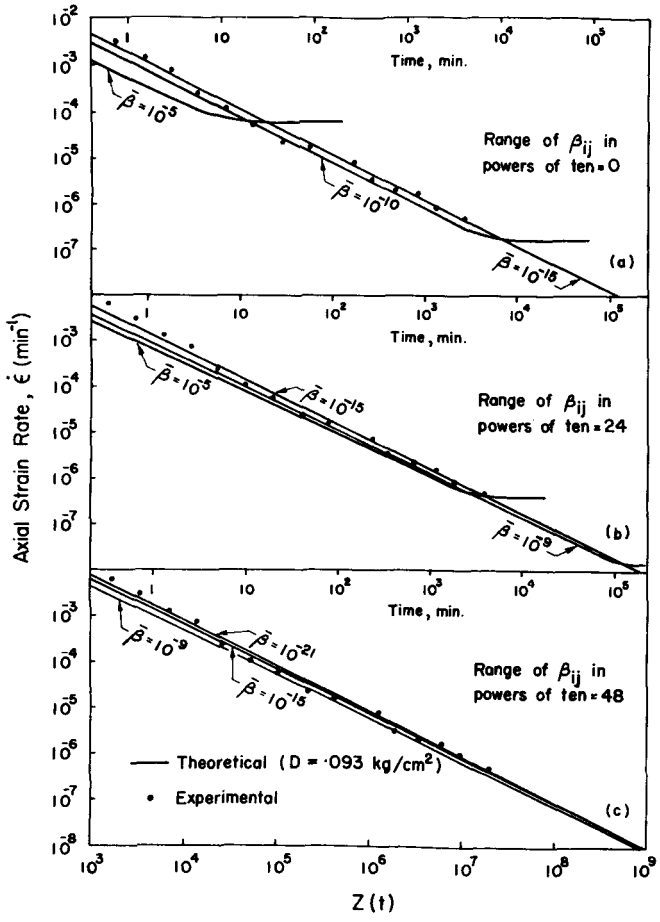



Fig. 8. Comparison of theoretical and experimental creep response.

stress level $\tau = 0{\cdot}043$ kg/cm$^2$. As in the case of the constant strain rate data, the sheet with the experimental data points was adjusted horizontally until the best fit was obtained. The agreement between the theoretical curves and the experimental results is excellent in the case of creep loading although some of the distributions shown are apparently unacceptable because their curves reach a steady-state condition while the experimental creep curves rarely exhibit such behavior.

The theoretical creep behavior predicted by the proposed model agrees well with the experimental behavior observed by Singh and Mitchell (1968) in that the slope of linear relationship between logarithm of strain rate and logarithm of time is nearly $-1$.

As in the case of constant strain rate, by matching the real time scale corresponding to the experimental points with the scale for the time parameter, $Z(t)$, the value of $Z(t)$ can be estimated. From the results shown in Fig. 8, it is found that

$$Z(t) \doteqdot 2500t \sim 4600t.$$

This value is, unfortunately, not in agreement with that obtained from constant strain rate loading. The value of $Z(t)$ from creep loading is approximately 13 times that obtained from constant strain rate. Although Fig. 8 shows the results of only one creep test, this ratio was quite consistent for all the tests performed in this investigation.

An explanation for the discrepancy between the constant strain rate and creep behavior is in order. In the first place, the response of the clay in constant strain rate loading may appear slower than it should because of seating problems, slack in the loading machinery, etc. Secondly, the material might strain-harden and become a stiffer material as loading progresses. Both of these effects can be handled by cyclic loading of the specimens until a



https://doi.org/10.1346/CCMN.1969.0170206 Published online by Cambridge University Press

consistent stress-strain curve is obtained. A small number of constant strain rate tests with cyclic loading has been recently performed. These tests show that

$$Z(t) \doteqdot 1000t \sim 3000t$$

which supports the foregoing explanation.

It is also possible that the theoretical model which, in order to be valid, requires that no significant structural changes occur during the deformation, may not be valid up to the ultimate stress. In most of the tests performed during this investigation, the steady-state condition was judged to have been reached at approximately 10 per cent strain. Strains of that magnitude may be beyond the limits of the validity of the theory.

## SUMMARY

A rheological model has been developed to describe the behavior of clays under load. The basic unit of deformation is assumed to consist of interparticle bond rupture occuring as a rate process plus the associated elastic deformation. The fundamental parameters of the model are identified as (1) the activation energy, $\Delta F_i$, (2) the macroscopic strain resulting from a bond rupture, $X_j$, (3) the elastic stiffness, $K_k$, and (4) the ratio of strain in a deformation unit to the macroscopic strain, $\Delta_l$. Owing to the heterogeneous nature of clay fabric, the concepts of distributed-parameters is introduced, in which the four fundamental model parameters are assumed to have a range of values which follow a normal distribution curve.

It is shown that the distributed-parameter model is capable of describing the constant strain rate and creep response of the clay tested. It is also shown that the distribution of the activation energy, $\Delta F_i$, has a dominating influence on the response of the model so that the distribution of the other parameters can be ignored for practical purposes. Although there is a discrepancy between the values of the time parameter $Z(t)$ as calculated from the constant strain rate and creep results, it is pointed out that this may be due, in part, to experimental difficulties.

*Acknowledgments*—Financial support for this investigation was provided by the National Science Foundation (Grant No. GK-657). The authors also wish to acknowledge the assistance of Mr. D. W. Schwoerer, who worked on the project in its early stages.

## REFERENCES

Christensen, R. W., and Wu, T. H. (1964) Analysis of clay deformation as a rate process. *J. Soil Mech. Found. Div., Am. Soc. Civil Engrs* **90**, No. SM6, Proc. Paper 4147, 125–157.

Eyring, H., and Halsey, G. (1948) The mechanical properties of textiles—the simple non-Newtonian model: *High Polymer Physics* (Edited by H. A. Robinson). Chem. Pub. Co., New York.

Geuze, E. C. W. A., and Tan, T. K. (1953) The mechanical behavior of clays: *Proc., 2nd Intern. Congr. Rheol, Oxford*, p. 247.

Glasstone, S., Laidler, K., and Eyring, H. (1941) *The theory of rate processes*: McGraw-Hill, New York.

Kauzmann, W. (1941) Flow of solid metals from the standpoint of the chemical-rate theory: *Trans. AIME* **143**, 57–83.

Mitchell, J. K. (1964) Shearing resistance of soils as a rate process: *J. Soil Mech. Found. Div., Am. Soc. Civil Engrs* **90**, No. SM1, Proc. Paper 3773, 29–61.

Mitchell, J. K. (1965) Closure to "Shearing resistance of soils as a rate process," *J. Soil Mech. Found. Div., Am. Soc. Civil Engrs* **91**, No. SM3, 106–114.

Mitchell, J. K., Campanella, R. G., and Singh, Awtar, (1968) Soil creep as a rate process: *J. Soil Mech. Found. Div. Am. Soc. Civil Engrs* **94**, No. SM1, Proc. Paper 5751, 231–253.

Murayama, S., and Shibata, T. (1958) On the rheological characteristics of clay, Part I: *Bull. 26*, Disaster Prevention Research Institute, Kyoto University, Japan.

Rosenquist, I. Th. (1959) Physical-chemical properties of soils: Soil water systems: *J. Soil Mech. Found. Div. Am. Soc. Civil Engrs* **85**, No. SM2, Proc. Paper 2000, 31–53.

Singh, Awtar, and Mitchell, J. K. (1968) General stress-strain-time function for soils: *J. Soil Mech. Found. Div. Am. Soc. Civil Engrs* **94**, No. SM1, Proc. Paper 5728, 21–46.

Tobolsky, A. V., Powell, R. E., and Eyring, H. (1943) Elastic-viscous properties of matter: *The Chemistry of Large Molecules*, Interscience, New York, p. 125.

West, Richard (1965) The characteristics of filter pressed kaolinite-water pastes: *Clays and Clay Minerals* **12**, 209–221.

**Résumé**—Le procédé de déformation des argiles est considéré comme une combinaison de déformation récupérable résultat du pliage et de la rotation des particules individuelles et de déformation irrécupérable due au mouvement relatif entre des particules adjacentes à leur point de contact. Le mouvement relatif est considéré comme un procédé progressif dans lequel les liaisons entre les particules sont brisées et rétablies de manière continue à mesure que la déformation avance. Il s'ensuit que le taux de déformation est gouverné par l'énergie d'activation associée à la rupture des liaisons entre les particules. En termes d'un modèle rhéologique, l'élément de base consiste en un ressort représentant la déformation récupérable en série avec un dashpot de taux représentant la déformation irréupérable.

En raison de la nature hétérogéneuse des sols d'argile, p.e. dimensions variables des particules,

https://doi.org/10.1346/CCMN.1969.0170206 Published online by Cambridge University Press

forme, orientation, caractéristiques de la surface etc., on s'attend à une gamme très large d'énergies d'activation, de rigidité élastique et d'autres caractéristiques. Cela est expliqué par l'hypothèse d'une distribution gaussienne des caractéristiques du modèle. Il s'ensuit que le modèle rhéologique complet postulé dans cette étude comporte une combinaison d'éléments de ressort et de dashpot couvrant la gamme totale des propriétés du modèle.

On analyse la réponse du modèle rhéologique du point de vue de la caractéristique de glissement et de charge à effort constant. L'analyse s'effectue par moyen numérique à l'aide d'un ordinateur numérique, étant donné qu'il n'existe aucune solution de forme fermée pour les systèmes non-linéaires d'équations résultant de ce modèle. Les données expérimentales pour un certain nombre d'essais à trois axes sur l'argile sous des conditions de charge différentes sont présentées en vue d'un comparaison avec le comportement du modèle.

**Kurzreferat** – Der Deformationsvorgang in Tonen wird als eine Kombination einer reversiblen Deformation, infolge der Biegung und Rotation von Einzelteilchen, und einer irreversiblen Deformation, infolge der Relativbewegung benachbarter Teilchen an ihren Beruhrungstellen, angesehen. Die Relativbewegung zwischen Teilchen wird als ein Geschwindigkeitsprozess behandelt, in welchem fortgesetzt Zwischenteilchenbindungen gebrochen und wieder hergestellt werden, u.zw. in dem Masse als der Deformationsvorgang fortschreitet. Demgemass wird die Deformationsgeschwindigkeit von der mit dem Bruch der Zwischenteilchenbindungen verknupften Aktivierungsenergie bestimmt. In der Ausdrucksweise eines rheologischen Modells bestünde also das grundlegende Element aus einer Feder, die die reversible Deformation wiedergibt und der ein Geschwindigkeitsprozess-Bremszylinder nachgeschaltet ist, der die irreversible Deformation darstellt.

Infolge des heterogenen Charakters des Tonbodengefüges, d.h. schwankende Teilchengrösse, Form, Orientierung, Oberflächenmerkmale usw., wird ein weiter Bereich von Aktivierungsenergien, elastischer Steife und sonstigen Werkstoffeigenschaften erwartet. Dieser Umstand wird Durch Annahme einer Gausschen Verteilung für die Modelleigenschaften berücksichtigt. Das in dieser Untersuchung vorgeschlagene, komplette, rheologische Modell besteht also aus einer Kombination von Feder- und Bremszylinderelementen, die den Gesamtbereich der Modelleigenschaften umfassen.

Die Reaktion des rheologischen Modells wird für Kriechverformung und Verformungsgeschwindigkeitsbelastung untersucht. Die Untersuchung wird zahlenmässig unter Vermendung eines Digitalrechners ausgeführt, da für die nichtlinearen Systeme von Gleichungen, die sich aus diesem Modell ergeben, keine Lösung geschlossener Form existiert. Es werden experimentelle Daten für eine Reihe triaxialer Prüfungen von Tonen unter verschiedenen Lastbedingungen zum zwecke eines Vergleichs mit dem Verhalten des Modells angeführt.

**Резюме**—Процесс деформации в глинах изображаем как сочетание поддающихся извлечению деформаций вследствие сгибания и вращения отдельных частиц и не поддающейся извлечению деформации из-за относительного движения между соседними частицами в точках их соприкосновения. Относительное движение между частицами рассматривается, как кинетический процесс, в котором межчастичные связи непрерывно прерываются и возобновляются по мере продвижения деформации. Соответственно скорость деформации определяется энергией активации, связанной с разрывом межчастичных связей. Таким образом, пользуясь понятиями реологической модели, основной элемент это пружина, представляющая восстанавливаемую деформацию, последовательно включенная с демпфером кинетического процесса, представляющим невосстанавливаемую деформацию.

Вследствие гетерогенных свойств структуры глинистых почв, т.е. разниц в размере частиц, форме, ориентации, поверхностных свойствах и т.п., предвидится широкий диапазон энергий активации, упругости и других существенных характеристик. Объясняется это, принимая распределение Гаусса для модельных свойств. Таким образом, укомплектованная реологическая модель, принимаемая для доказательств в настоящем исследовании, состоит из пружины и демпфера, покрывая весь спектр модельных свойств.

Реагирование реологической модели подвергается анализу на ползучесть и постоянное напряжение—степень нагрузки. Анализ выполняется цифрово, пользуясь цифровой вычислительной машиной, так как не существует решения предопределенной формы для нелинейных систем уравнений, результирующих из этой модели. Экспериментальные данные, полученные из ряда трехосных испытаний на глине в различных условиях нагрузки, представлены здесь для сравнения с поведением модели.

https://doi.org/10.1346/CCMN.1969.0170206 Published online by Cambridge University Press